JOM Journal of Optical Microsystems

RESEARCH PAPER

Solution-based Sb_2Se_3 thin films for microphotonics

Rashi Sharma,[a,*] Casey Schwarz,[b] Daniel Wiedeman,[c] Eric T. S. Bissell,[d] Brian Mills,[e,f] Marie Sykes,[b] Jasper Stackawitz,[b] Jake Klucinec,[b] Dennis Callahan,[g] JueJun Hu,[e] Parag Banerjee,[d] and Kathleen Richardson[a]

[a]University of Central Florida, CREOL, The College of Optics & Photonics, Orlando, Florida, United States
[b]Ursinus College, Department of Physics and Astronomy, Collegeville, Pennsylvania, United States
[c]University of Central Florida, Department of Chemistry, Orlando, Florida, United States
[d]University of Central Florida, Department of Materials Science and Engineering, Orlando, Florida, United States
[e]Massachusetts Institute of Technology, Department of Materials Science and Engineering, Cambridge, Massachusetts, United States
[f]Draper Scholar Program, Charles Stark Draper Laboratory Inc., Cambridge, Massachusetts, United States
[g]Charles Stark Draper Laboratory Inc., Cambridge, Massachusetts, United States

ABSTRACT. The development of functional chalcogenide optical phase change materials holds significant promise for advancing optics and photonics applications. Our comprehensive investigation into the solution processing of Sb_2Se_3 thin films presents a systematic approach from solvent exploration to substrate coating through drop-casting methods and heat treatments. By employing characterization techniques such as scanning electron microscopy, dynamic light scattering, energy-dispersive X-ray spectroscopy, Raman spectroscopy, and X-ray diffraction, we reveal crucial insights into the structural, compositional, and morphological properties of the films as well as demonstrated techniques for control over these features to ensure requisite optical quality. Our findings, compared with currently reported deposition techniques, highlight the potential of solution deposition as a route for scalable Sb_2Se_3 film processing.

Keywords: phase change materials; solution-derived chalcogenides; chalcogenide thin films; phase transitions; optical properties

Paper 23041SS received Dec. 29, 2023; revised Mar. 2, 2024; accepted Apr. 2, 2024; published May 25, 2024.

1 Introduction

Phase change materials (PCMs) are a type of chalcogenide media that are capable of undergoing dramatic property changes upon structural transformation from their amorphous to crystalline states.[1–4] PCMs are widely known for their ability to store information through this reversible transition between their amorphous and crystalline phases, which can be triggered by external factors, such as heat, electric current, or optical pulses.[1] PCMs, largely the compositions $Ge_2Sb_2Te_5$ (GST) and $Ag_xIn_ySb_2Te$ (AIST),[1,5] have been used in applications including optical data storage and electronic memories. However, these common PCMs exhibit a large absorption loss in one or both states, which limits their functionality and overall use in optical device applications, such as in microphotonic circuits.[6,7] PCMs for such devices are typically referred to as optical PCMs (O-PCMs).

*Address all correspondence to Rashi Sharma, Rashi.Sharma@ucf.edu

New PCM compositions, including the chalcogenide alloy compositions $Ge_2Sb_2Se_4Te$, Sb_2S_3, Sb_2Se_3, $Ge_2Sb_2Te_3S_2$, and In_3SbTe_2, have been developed as low-loss alternatives, specifically tailored for use in such photonic applications.[8–13] Here, we focus on antimony triselenide (Sb_2Se_3) as a low-loss, reversible alternative to commercially available PCMs.[10] Sb_2Se_3 was first studied about 60 years ago for its use in thermoelectric semiconductors.[14,15] More recently, Sb_2Se_3 has been investigated as a solar cell absorber material due to its bandgap energy of 1.2 eV, yielding strong absorption in the visible region.[15,16] Sb_2Se_3 has a reported high refractive index contrast of $\Delta n = 0.77$ at $\lambda = 1.55$ μm[15] and low loss, which makes it a unique PCM candidate for telecommunications, metamaterials structures, integrated nanophotonics in the infrared region.[4,9,10,17] These studies have focused on Sb_2Se_3 films deposited by physical vapor deposition (PVD) techniques, such as thermal evaporation and radio frequency (RF) sputtering.[15,18–23]

Solution processing offers a cost-effective, large-area, and scalable alternative to PVD for chalcogenide thin film deposition. Solution deposition of chalcogenide glass (ChG) films is a well-practiced technique dating back to the 1980s, mostly centered on As-Se-S-Sb-Ge–based materials and other ChGs.[24–30] Since then it has been used to create waveguides, photonic crystals, and micro-lenses as well as other optical components.[31–36] However, reports on solution-processed chalcogenide PCMs have been scarce to date[8,37–40] and their applications in optical devices have not been explored, to the best of our knowledge.[41,42]

In this paper, we report solution deposition as a potentially low-cost, large-area, scalable coating technique for the O-PCM Sb_2Se_3. We detail the solution processing of Sb_2Se_3 thin films from solvent exploration to substrate coating, heat treatments, and resultant film quality. When referring to the prepared alloy and solvent mixture, we use the term "ink," and when referring to a film that has gone through the baking and evaporation processes and remains on the substrate, we use the term "solution-derived (SD)" films. Dynamic light scattering (DLS) was used to measure the particle/aggregate size of Sb_2Se_3 in the prepared ink solution prior to deposition. SD Sb_2Se_3 films are then characterized using white light interferometer (WLI), scanning electron microscopy (SEM), energy-dispersive X-ray spectroscopy (EDS), Raman spectroscopy, and X-ray diffraction (XRD). These tools provide insights into the film's structural, compositional, and morphological properties and enable the correlation of processing conditions with resulting properties and functionalities. This work not only contributes to the advancement of PCMs for photonics applications but also demonstrates a systematic approach to the fabrication, processing, and characterization of SD PCM films.

2 Solution Processing and Drop Cast Methods

2.1 Alloy Formation

Boules of Sb_2Se_3 were prepared by a melt quenching technique. High purity (4N) antimony (Sb), and sulfur (S) (Alfa Aesar) were stored in a glove box under a controlled atmosphere ($H_2O < 1$ ppm and $O_2 < 0.1$ ppm). Alloy elemental materials were batched in a silica ampoule, which was then sealed under vacuum (10^{-2} Torr) with a hydrogen/oxygen torch. The ampoule was then placed in a rocking furnace and heated 750°C for 12 h. After the dwell period, the glass was air-quench at 650°C. The alloy was crushed in a ball mill for 2 h and subsequently sieved (75 μm) using an ultrasonic sieving system (MTI Corporation) in a glove box.

2.2 Precursor Solution

Precursor solutions were prepared in a nitrogen-filled glove box (H_2O and $O_2 < 0.1$ ppm) to prevent surface oxidation of the deposited film. Sb_2Se_3 precursor inks with 1.0 wt. % loading levels of alloy in solvent were prepared in a 9:1 ethylene diamine (EDA) and ethane thiol (EtSH) solution mixture by stirring at room temperature for 30 min. This solution chemistry has been successfully applied to a wide array of chalcogenide compositions.[26,43–45] The resulting Sb-Se ink was stable at room temperature and deemed not photosensitive. A control experiment showed that Sb_2Se_3 possesses negligible solubility toward EDA alone in the absence of EtSH, defining the solvent mixture chosen for ink solutions. The films were prepared by drop-casting (20 μl) Sb_2Se_3 ink onto a TiO_2 (4 nm) coated Si wafer. A TiO_2-coated Si wafer was chosen as a substrate as such coating exhibited improved wettability of the solvent as compared to Si wafers alone. For transmission measurements, Sb_2Se_3 ink (5 μl) was deposited onto a ZnSe substrate for infrared

transmission tests. The drop-casted film was soft baked at 50°C for 20 min, followed by a hard bake at 190°C for 2 h to produce Sb_2Se_3 thin films. The two-step heat treatment has been shown in prior work to reduce pinholes and cracking in rapidly evaporated films, which are detrimental to the resulting film's optical quality.[30]

2.3 Material Characterization

The soft and hard-bake protocols were determined by monitoring the rate of solvent evaporation from an ink-coated ZnSe substrate using a ThermoFisher Nicolet IS5 FTIR spectrometer. WLI Zygo NewView 8000 was used to measure film thickness and roughness upon heat treatment to quantify how processing affects film properties. A Zeiss Ultra 55 FEG scanning electron microscope (SEM) was used to study film morphology and film thickness on the SD Sb_2Se_3 thin films prepared on TiO_2-coated Si wafer. The Thermo Scientific Noran System 7 electron dispersive spectroscopy (EDS) was used to identify the elemental composition of the film. A Malveran Zetasizer Nano ZSZEN 3600 DLS instrument with a particle detection range of 0.3 nm to 10 μm was used to measure the particle size of Sb_2Se_3 molecular clusters in the ink. XRD characterization of the thin films was done by grazing incidence with a PANalytical Empyrean system with a sealed Cu Kα tube with an incidence angle at $\omega = 2$ deg at room temperature. Raman characterization (Horiba LabRam HR Evolution Nano) was performed on reference thermally evaporated (TE) and SD films of Sb_2Se_3 in air at $\lambda = 532$ nm to investigate film chemical structure. Figure 1 shows the overall preparation method of Sb_2Se_3 thin films via the drop-casting technique.

3 Results and Discussion

3.1 Solvent Evaporation

The Sb_2Se_3 ink (5 μl) was drop-casted on a cleaned ZnSe substrate to ascertain the maximum temperature and time required for complete solvent evaporation. Residual solvent in PCM films leads to undesirable absorption loss at bands associated with solvent-chemistry bonds, in the infrared. The extent of solvent evaporation was measured by monitoring the disappearance of the solvent (EDA and EtSH) absorption peaks with temperature and time. It is easy to discern preferential evaporation since EDA absorption peaks are observed at $\lambda = 6.27$, 11.48, and 12.3 μm, whereas in EtSH peaks are at $\lambda = 3.37$, 6.9, 7.78, 10.5, and 13.3 μm. Figure 2 shows the transmission spectra of the ink-coated ZnSe substrate baked under different times/temperatures. It was noted that multi-solvent solutions such as those made in this study from EDA and EtSH possess slightly different (preferential) evaporation rates. Hence, one might expect variation in the decrease in absorption bands associated with respective solvent signatures as seen here. The majority of the solution (comprised primarily of EDA) was evaporated during the first

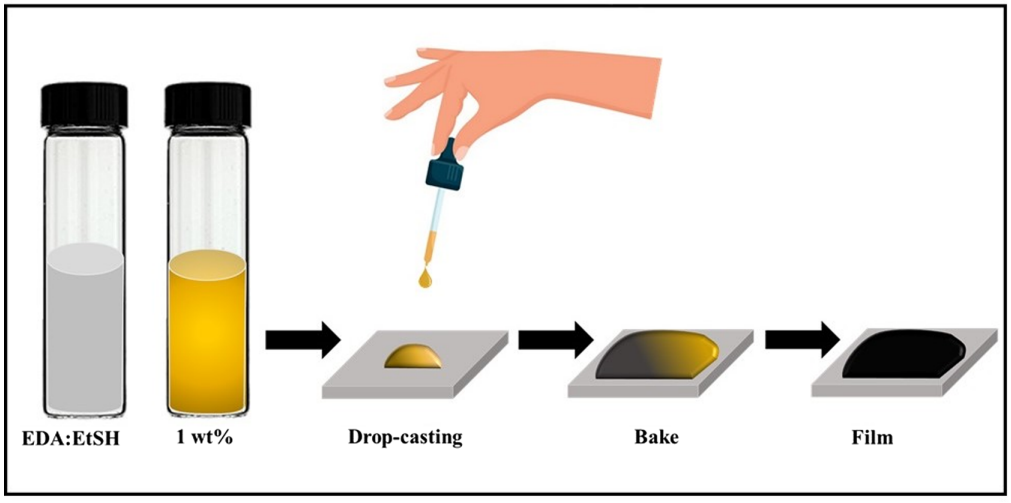

Fig. 1 Illustration of the Sb-Se precursor solution in 9:1 EDA: EtSH solution and the preparation of Sb_2Se_3 films.

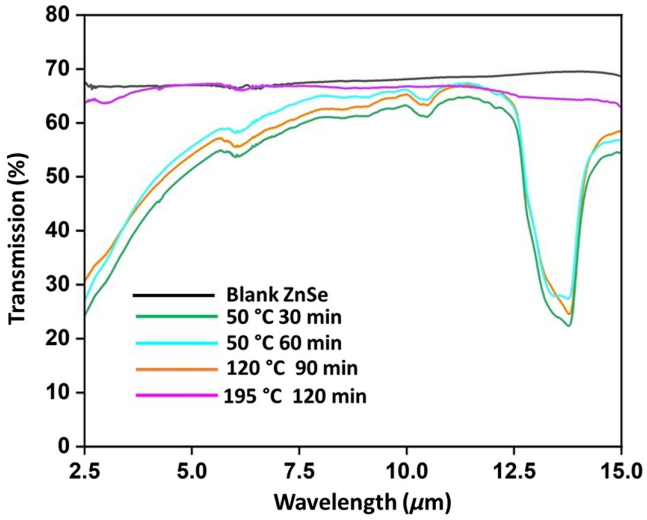

Fig. 2 Transmission measurements of film deposited on ZnSe substrate as a function of bake protocol.

soft-bake protocol at 50°C for 30 min. Higher temperatures were needed for the thiol-containing solvent. Further baking of the film from 50°C to 120°C for up to 90 min did not result in complete evaporation of the thiol as represented by the presence of peaks at $\lambda = 10.5$ and 13.3 μm as well as the scattering tail toward lower wavelengths. The short-wavelength tail may be due to heat-treatment-induced (partial) crystallization of the film or evidence of small-scale particle clusters that were not sufficiently eliminated with heat treatment, which results in scatter loss. Hard-baking the film at 195°C for 2 h allowed complete film consolidation, resulting in full evaporation of the solvent, therefore confirming the necessary temperature at which the substrate should be baked. The lack of scatter tail in the final hard-baked film is indicative of the merging of the molecular droplet with heat treatment and their scatter, shown at shorter times/low temperatures, goes away with heat treatment. In the case of a film with high (~15 to 20 μl) drop casted volume, the final film will likely show a scatter tail associated with incomplete film formation.

3.2 Surface Measurements and Particle Size

Since the ultimate goal of this work is to integrate the Sb_2Se_3 thin films onto photonic devices exemplified by silicon-on-insulator (SOI) waveguides (possibly coated with a TiO_2 layer as needed), from this point onward we continue our work on TiO_2 coated Si wafers instead of ZnSe as the substrate in a glove box. Figure 3 shows the surface morphology details of the films

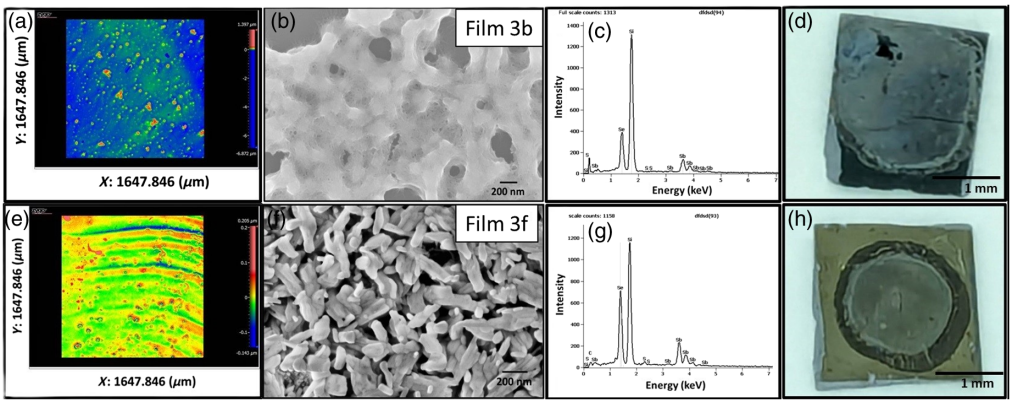

Fig. 3 (a) WLI image of the center of the film baked at 175°C. (b) SEM image of film baked at 175°C, (c) EDS measurements of film 3b baked at 175°C (scale bar 200 nm), (d) optical image of the film 3b dropcasted on Si wafer (scale bar 1 mm), (e) WLI image of the center of the film baked at 190°C, (f) SEM image of the film baked at 190°C (scale bar 200 nm), (g) EDS measurements of film 3f baked at 190°C, and (h) optical image of the film 3f dropcasted on Si wafer (scalebar 1 mm).

as a function of the hard-bake protocol. The film displayed in Fig. 3(a) was hard-baked at 175°C for 2 h whereas the film displayed in Fig. 3(e) was hard-baked at 190°C for 2 h. Figures 3(a) and 3(e) show WLI images of the center of the films with an average root-mean-square (RMS) roughness of 132 and 23 nm, respectively. SEM images of films 3a and 3e are shown in Fig. 3(b) (we will call this film 3b) and Fig. 3(f) (we will call this film 3f), respectively. SEM images revealed that for film 3b, despite solvent removal, the resulting alloy film is not uniform. Here, one can observe an interconnected network of the particles and evidence of porosity exhibiting a thick mesh-like structure comprised of relatively large gaps down to the substrate. Contrarily, segregated particles of Sb_2Se_3 (diameters of $\sim 280 \pm 50$ nm) were visualized in film 3f, and the gaps were smaller with increased homogeneity.

The EDS spectra revealing elemental compositions of the films are shown in Fig. 3(c) (for film 3b) and Fig. 3(g) (for film 3f). As it can be seen, the presence of a small percentage of sulfur (2.5 at. %) due to incomplete evaporation of thiol (resulting in soft film) is the reason behind the aggregation in film 3b. On the other hand, hard-baking the film to 190°C resulted in complete evaporation of the solvent as shown in Fig. 3(f).

In film 3f, particles with an average length ($\sim 280 \pm 50$ nm) were observed. To further understand the aggregation/agglomeration of Sb_2Se_3 in the film, we analyzed the ink using DLS. The analysis was done at $\lambda = 632$ nm with 1 wt. % Sb_2Se_3 dissolved in the ratio of EDA:EtSH (9:1). Figure 4 shows a plot of intensity versus particle size. Here, Sb_2Se_3 was dissolved in solution and measured at room temperature; this resulted in an average particle size of 260 nm, which was close to the particle size observed in film 3f. These data support the prior evidence that shows that with the soft and hard bake protocol of 50°C for 20 min and 190°C for 2 h the particles did not aggregate fully. To further study the impact of temperature on the particle size, 1 wt. % Sb_2Se_3 was dissolved in EDA:EtSH at 50°C for 20 min followed by DLS measurement. Figure 4 shows that the average particle size of Sb_2Se_3 in the ink reduced from ~ 260 to ~ 110 nm upon being dissolved at an elevated temperature of 50°C. To confirm this observation, 20 μl Sb_2Se_3 (also dissolved at 50°C) was drop-casted and dried on Si substrate and imaged via SEM. Figure 4 inset image shows the SEM of the film with an average particle length of 150 ± 30 nm, confirming the results of the DLS.

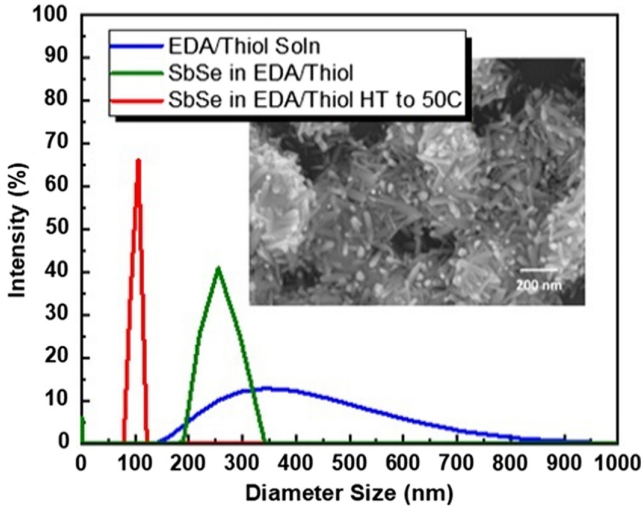

Fig. 4 DLS measurements of the average particle size of Sb_2Se_3 in the ink dissolved at 50°C with inset SEM image of the film. The spectrum of the pristine EDA:EtSH (9:1) solution (blue line) with no dissolved Sb_2Se_3 material shows a wide range of particulates with an average peak at 350 nm. The spectrum of the 1 wt. % Sb_2Se_3 dissolved in the ratio of EDA:EtSH (9:1) (green line) dissolved and measured at room temperature resulted in an average particle size of 260 nm. The spectrum of the 1 wt. % Sb_2Se_3 dissolved in the ratio of EDA:EtSH (9:1) (red line) dissolved at an elevated temperature of 50°C showed a reduction in average particle size down to 110 nm. The inset SEM image is of a film created using 1 wt. % Sb_2Se_3 dissolved at an elevated temperature of 50°C in the ratio of EDA:EtSH (9:1). This film depicts crystallites with an average particle diameter 150 nm, confirming the DLS measurements.

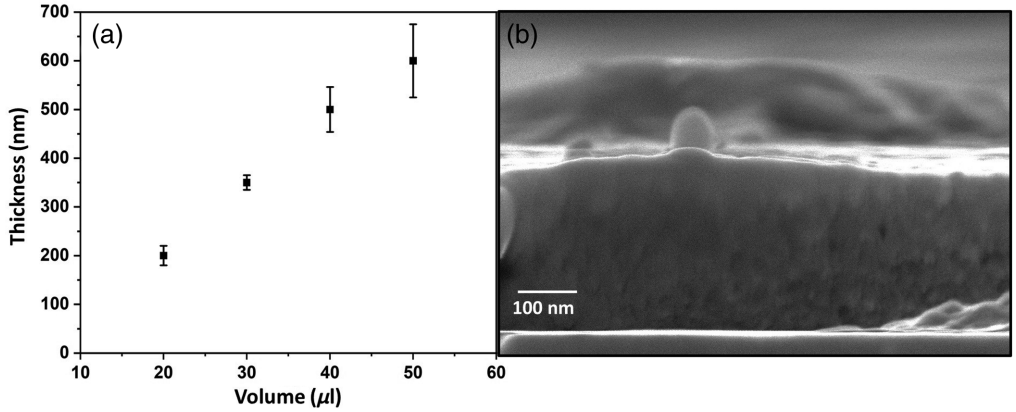

Fig. 5 (a) Post heat treated Sb_2Se_3 film thickness (nm) versus drop casted volume (μl) and (b) SEM image of film cross-section of a 200 nm thick film (scale bar 100 nm).

3.3 Film Thickness

An important factor in incorporating the SD films for photonic applications is the ability to control thickness as a parameter. Film thickness depends not only on the loading levels of the alloy (Sb_2Se_3) in the solvent mixture but also on the drop-casted volume of the ink deposited onto the substrate prior to solvent evaporation. Following an investigation to evaluate optimal loading levels, different volumes of the 1 wt. % Sb_2Se_3 ink were drop-casted on Si substrates and dried using the soft- and hard-bake protocol described above. The plot in Fig. 5(a) shows a plot of film thickness versus drop-casted volume. Here, the resulting, post-heat treat film thickness ranges from 200 to 500 nm; Fig. 5(b) shows an SEM image of the cross-sectional side view of the film with ~200 nm thickness.

3.4 X-Ray Diffraction and Raman Spectra

The SD-derived films were further evaluated via XRD and Raman spectroscopy followed by comparison with the films deposited via thermal evaporation. The TE films were deposited from a stoichiometric powdered Sb_2Se_3 source in a custom deposition system. Films are deposited at a pressure of 10^{-6} Torr and substrate temperatures are monitored to be about 40°C.[46–48] To confirm the presence of Sb_2Se_3 *in situ* XRD measurements were performed on film 3b and film 3f at room temperature [Fig. 6(a)], following solvent removal via the heat treatment protocols noted above. The XRD of the SD films were then compared with the TE as-deposited and annealed (190°C for 2 h) films of the Sb_2Se_3 alloy. The as-deposited TE films were amorphous in nature whereas the TE annealed film was crystalline. The films deposited at 175°C were also found to be

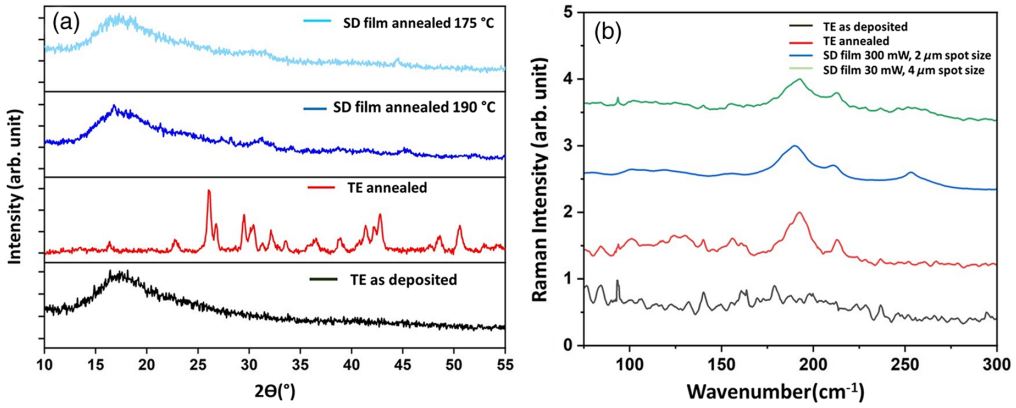

Fig. 6 (a) XRD measurements of film 3b (175°C) and film 3f (190°C) and comparison of the peaks with TE as-deposited and annealed films, (b) Raman spectra of the TE amorphous and annealed films (measured at 300 mW, 2 μm spot size), and comparison with SD Sb_2Se_3 film measured at different powers.

predominantly amorphous in nature, and as was discussed above due to incomplete evaporation of solvent in this film. Film deposited at 190°C contained a mixture of amorphous and crystalline peaks. The predominant peaks of crystalline Sb_2Se_3 were observed in the post-heat-treated film at 2θ values of 16.874 deg, 31.160 deg, and 32.220 deg.[34] The presence/absence of some crystallization peaks in the film baked at 190°C confirms that the film undergoes crystallization during the hard baking process which is an important step to ensure complete solvent evaporation. No additional peaks were found during the solvent evaporation process that would correspond to the detection possible oxidation of Sb_2Se_3 into Sb_2O_5 or Sb_2O_3 peaks.

Raman measurements were performed on both TE and SD films (300 mW, 2 μm spot size), in order to confirm the presence of Sb_2Se_3 in the SD film. The Raman spectrum for the as-deposited TE film showed no distinct peaks recognized over noise. For both the TE and SD annealed films, the Raman spectra displayed peaks at 191 and 210 cm^{-1}, these peaks are commonly assigned to the Sb_2Se_3 phase, particularly the A_g mode of the Sb–Se–Sb bending vibrations of Sb_2Se_3.[49] Having these two peaks present in both the TE and SD films indicates common structural development occurring during annealing of both films regardless of processing. It should be noted that no lower frequency peaks were observed in the as-deposited or annealed TE or SD Sb_2Se_3 films in our study. This is likely be due to differences in processing, heat treatments, annealing, and interaction volume, between our film and the references. For both peaks at 191 and 210 cm^{-1}, the full-width at half-maximum for the annealed SD films is almost twice (~24 cm^{-1} compared to ~40 cm^{-1}) than that of the annealed TE films, indicating reduced crystallinity for the SD films, as was also confirmed via XRD. In the SD film, a new peak at 255 cm^{-1} emerged, this peak was assigned to Sb_2O_3 and indicated that the Raman laser interaction with the film induced further annealing which resulted in oxidation of the film.[49] The Sb_2O_3 peak at 255 cm^{-1} did not form when the SD film was remeasured at a lower power of 30 mW with 4 μm spot size. The SD films appear to be more sensitive to oxidation than the TE film. Future Raman characterization will need to take this oxidation behavior into account. It may be necessary to perform Raman under an inert N_2 atmosphere to prevent oxidation during measurement.

4 Silicon on Insulator Microheaters

Recently, we have reported using silicon-on-insulator (SOI) microheater arrays as a multifunctional platform capable of characterizing the structural, optical, kinetic, thermal, and cycling behavior of optical PCMs.[12] We have shown the platform's capability to conduct *in situ*, quantitative analyses of various aspects of PCM thin films, including phase composition, optical constants, temperature profiles, time-temperature-transformation diagrams,[13] cycling endurance, and material uniformity.

A combination of the micro-heater platform with the SD film processing described herein presents intriguing opportunities for new PCM discovery and process development. The microheater platform can be integrated with combinatorial solution deposition techniques, such as inkjet printing methods, streamlining the process of high-throughput screening for new compositions of PCMs. Its *in situ* characterization capabilities also facilitate efficient screening of heat treatment conditions of SD PCM films, similar to what we presented in Sec. 3 but with much-enhanced throughput. The large-area scalable SD technique is also commensurate with the wafer-scale micro-heater platform. Our next step will involve exploring the deposition and characterization of SD films on the SOI micro-heaters.

5 Conclusions

In conclusion, this study delves into the exploration of Sb_2Se_3 SD thin films as a low-loss alternative for PCMs in optical applications. The unique properties of Sb_2Se_3, including its high refractive index contrast, low toxicity, and bandgap energy, make it a promising candidate for integrated nanophotonics. This paper details the comprehensive solution processing of Sb_2Se_3 thin films, addressing key aspects, such as film morphology, composition, and thickness control via loading levels, the drop-casting volume as well as the impact of baking temperature on the film morphology. XRD analysis of the films revealed the change in intensity of Sb_2Se_3

crystallization peaks as the hard bake temperature for the solvent evaporation is increased from 175°C to 190°C. Further analysis of this film via *in situ* XRD from room temperature to 400°C under an inert atmosphere will be done in future work. Raman analysis of the SD films and their comparison with the well-studied TE films showed peaks at 191 and 210 cm^{-1} which are commonly assigned to Sb_2Se_3. The formation of Sb_2O_3 at 255 cm^{-1} revealed the sensitivity of the SD films to air. The SD films were much more sensitive to oxidation than TE films. The findings not only contribute to advancing optical PCMs but also provide a new alternative to conventional PVD methods for the fabrication, processing, and characterization of Sb_2Se_3 PCM films.

Disclosures

The authors report no conflicts of interest.

Code and Data Availability

The sample was created in-house using a melt-quench technique with commercially available elemental materials. The drop-casting technique has been clearly illustrated here as well as in other references. The fabrication of microheater array devices is achievable through established photonic foundry services, and the hardware and software designs of the characterization platform are publicly accessible.

Acknowledgments

Funding support was provided by NSF (Grant Nos. 2132929, 2225968, and 2225967). Dr. Schwarz acknowledges support provided from Ursinus College's faculty flex funding, research grant and the Pearlstine Faculty Fellowship Award. B. Mills acknowledges support provided by the Draper Scholar Program.

References

1. S. Raoux et al., "Phase change materials and phase change memory," *MRS Bull.* **39**, 703–710 (2014).
2. Z. Wang et al., "Resistive switching materials for information processing," *Nat. Rev. Mater.* **5**, 173–195 (2020).
3. S. Wei, P. Lucas, and C. A. Angell, "Phase-change materials: the view from the liquid phase and themetallicity parameter," *MRS Bull.* **44**, 691–698 (2019).
4. Z. Fang, "Non-volatile programmable photonics based on phase change materials," University of Washington (2023).
5. W. Zhang et al., "Designing crystallization in phase-change materials for universal memory and neuro-inspired computing," *Nat. Rev. Mater.* **4**, 150–168 (2019).
6. R. E. Simpson, J. K. W. Yang, and J. Hu, "Are phase change materials ideal for programmable photonics? Opinion," *Opt. Mater. Express* **12**, 2368–2372 (2022).
7. D. Tripathi et al., "Recent developments in chalcogenide phase change material-based nanophotonics," *Nonotechnology* **34**, 502001 (2023).
8. C. L. Hassam et al., "Robust, transparent hybrid thin films of phase-change material Sb_2S_3 prepared by electrophoretic deposition," *ACS Appl. Energy Mater.* **4**, 9891–9901 (2021).
9. M. Delaney et al., "Nonvolatile programmable silicon photonics using an ultralow-loss Sb_2Se_3 phase change material," *Sci. Adv.* **7**, eabg3500 (2021).
10. W. Jia, R. Menon, and B. Sensale-Rodigue, "Unique prospects of phase change material Sb_2Se_3 for ultra-compact reconfigurable nanophotonic devices," *Opt. Mater. Express* **11**, 3007–3014 (2021).
11. C. Rios et al., "Phase change materials for optics and photonics: feature issue introduction," *Opt. Mater. Express* **12**, 4284–4286 (2022).
12. C. Popescu et al., "An open-source multi-functional testing platform for optical phase change materials," *Small Sci.* **3**, 2300098 (2023).
13. S. A. Vitale et al., "Phase transformation and switching behavior of magnetron plasma sputtered $Ge_2Sb_2Se_4Te$," *Adv. Photonics Res.* **3**, 2200202 (2022).
14. G. Voutsas et al., "The crystal structure of antimony selenide, Sb_2Se_3," *Zeitschr. Kristallogr.-Crystal. Mater.* **171**, 261–268 (1985).
15. M. Delaney et al., "A new family of ultralow loss reversible phase-change materials for photonic integrated circuits: Sb_2S_3 and Sb_2Se_3," *Adv. Funct. Mater.* **30**, 2002447 (2020).
16. T. Ju et al., "Enhanced photovoltaic performance of solution-processed Sb_2Se_3 thin film solar cells by optimizing device structure," *Curr. Appl. Phys.* **20**, 282–287 (2020).

17. C. Ríos et al., "Ultra-compact nonvolatile phase shifter based on electrically reprogrammable transparent phase change materials," *PhotoniX* **3**, 26 (2022).
18. D. Lawson et al., "Time-resolved reversible optical switching of the ultralow-loss phase change material Sb_2Se_3," *J. Opt.* **24**, 064013 (2022).
19. D. S. Cuz et al., "Structural, optical and morphological characterization of Sb_2S_3 thin films grown by physical vapor deposition," in *18th Int. Conf. Electr. Eng., Comput. Sci. and Autom. Control (CCE)*, Mexico City, Mexico (2021).
20. R. Jakomin et al., "Advances on Sb_2Se_3 solar cells fabricated by physical vapor deposition techniques," *Solar* **3**, 566–595 (2023).
21. A. Dutta et al., "Tunable optoelectronic properties of radio frequency sputter-deposited Sb_2Se_3 thin films: role of growth angle and thickness," *Sol. Energy* **194**, 716–723 (2019).
22. Y.-Z. Li et al., "Sb_2Se_3 thin films fabricated by thermal evaporation deposition using the powder prepared via mechanical alloying," *Surf. Coat. Technol.* **358**, 1013–1016 (2019).
23. A. H. H. Al-Obeidi and B. K. H. Al-Maiyaly, in *1st Diyala Int. Conf. for Pure and Appl. Sci.: ICPAS2021, AIP Conf. Proc.*, Vol. 2593 (2023).
24. G. C. Chern and I. Lauks, "Spin coated amorphous chalcogenide films: structural characterization," *J. Appl. Phys.* **54**, 2701–2705 (1983).
25. Y. Zha, M. Waldmann, and C. B. Arnold, "A review on solution processing of chalcogenide glasses for optical components," *Opt. Mater. Express* **3**, 1259 (2013).
26. C. McCarthy et al., "Solution-phase conversion of bulk metal oxides to metal chalcogenides using a simple thiol-amine solvent mixture," *Angew. Chem.* **127**, 8498–8501 (2015).
27. S. Song et al., "Spin-coating of $Ge_{23}Sb_7S_{70}$ chalcogenide glass thin films," *J. Non-Cryst. Solids* **355**, 2272–2278 (2009).
28. Y. Zou et al., "Solution processing and resist-free nanoimprint fabrication of thin film chalcogenide glass devices: inorganic-organic hybrid photonic integration," *Adv. Opt. Mater.* **2**, 759–764 (2014).
29. S. Slang et al., "Mechanism of the dissolution of As–S chalcogenide glass in n-butylamine and its influence on the structure of spin coated layers," *J. Non-Cryst. Solids* **426**, 125–131 (2015).
30. J. Wilkinson, "Characterization and optimization of solution-derived chalcogenide thin films," Clemson University (2012).
31. H. Khan et al., "Solution processing of chalcogenide glasses: a facile path towards functional integration," *Opt. Mater.* **119**, 111332 (2021).
32. C. Tsay, Y. Zha, and C. B. Arnold, "Solution-processed chalcogenide glass for integrated single-mode mid-infrared waveguides," *Opt. Express* **18**, 26744–26753 (2010).
33. Y. Zha et al., "Inverted-rib chalcogenide waveguides by solution process," *ACS Photonics* **1**, 153–157 (2014).
34. C. Tsay et al., "Mid-infrared characterization of solution-processed As_2S_3 chalcogenide glass waveguides," *Opt. Express* **18**, 15523 (2010).
35. N. Carlie et al., "Integrated chalcogenide waveguide resonators for mid-IR sensing: leveraging material properties to meet fabrication challenges," *Opt. Express* **18**, 26728 (2010).
36. J. W. Choi et al., "Nonlinear characterization of GeSbS chalcogenide glass waveguides," *Sci. Rep.* **6**, 39234 (2016).
37. Y. R. Wang et al., "Electronic and optical switching of solution-phase deposited $SnSe_2$ phase change memory material," *J. Appl. Phys.* **109**, 113506 (2011).
38. A. Simon et al., "Introduction of chalcogenide glasses to additive manufacturing: nanoparticle ink formulation, inkjet printing, and phase change devices fabrication," *Sci. Rep.* **11**, 14311 (2021).
39. D. B. Mitzi et al., "Solution-based processing of the phase-change material KSb_5S_8," *Chem. Mater.* **18**, 6278–6282 (2006).
40. P. N. Bartlett et al., "Non-aqueous electrodeposition of functional semiconducting metal chalcogenides: $Ge_2Sb_2Te_5$ phase change memory," *Mater. Horiz.* **2**, 420–426 (2015).
41. V. M. Koch et al., "Sb_2Se_3 thin-film growth by solution atomic layer deposition," *Chem. Mater.* **34**, 9392–9401 (2022).
42. D. Milliron, S. Raoux, and R. Shelby, "Solution-phase deposition and nanopatterning of GeSbSe phase-change materials," *Nat. Mater.* **6**, 352–356 (2007).
43. C. L. McCarthy and R. L. Brutchey, "Solution processing of chalcogenide materials using thiol–amine "alkahest" solvent systems," *Chem. Commun.* **53**, 4888–4902 (2017).
44. D. H. Webber et al., "Facile dissolution of selenium and tellurium in a thiol–amine solvent mixture under ambient conditions," *Chem. Sci.* **5**, 2498–2502 (2014).
45. D. H. Webber and R. L. Brutchey, "Alkahest for V_2VI_3 chalcogenides: dissolution of nine bulk semiconductors in a diamine-dithiol solvent mixture," *J. Am. Chem. Soc.* **135**, 15722–15725 (2013).
46. C. J. Zhang et al., "Broadband transparent optical phase change materials for high-performance nonvolatile photonics," *Nat. Commun.* **10**, 4279 (2019).

47. J. Hu et al., "Fabrication and testing of planar chalcogenide waveguide integrated microfluidic sensor," *Opt. Express* **15**, 2307–2314 (2007).
48. J. D. Musgraves et al., "Comparison of the optical, thermal and structural properties of Ge–Sb–S thin films deposited using thermal evaporation and pulsed laser deposition techniques," *Acta Mater.* **59**, 5032–5039 (2011).
49. A. Kumar et al., "Raman spectroscopy and *in situ* XRD probing of the thermal decomposition of Sb_2Se_3 thin films," *J. Phys. Chem. C* **125**, 19858–19865 (2021).

Rashi Sharma is a postdoctoral scientist at the University of Central Florida (UCF) in Orlando, Florida, working in CREOL, the College for Optics and Photonics. She received her PhD in chemistry from the UCF in 2018. She is the author of 14 journal papers and has written one book chapter. Her current research interests include engineering of IR transparent glass and glass ceramics. She is a member of SPIE.

Casey Schwarz is an associate professor of physics and chair of the Physics and Astronomy Department at Ursinus College in Collegeville, Pennsylvania. She received her PhD in physics from the UCF in 2012 and served as a postdoctoral scholar in chemistry and CREOL, the College for Optics and Photonics at UCF. Her research interests include laser writing of new materials, the development and design of optical devices, bioactive glasses, and undergraduate education.

Biographies of the other authors are not available.